Kinetics of the Light and Elevated Temperature Induced Degradation and Regeneration of Quasi-Monocrystalline Silicon Solar Cells

Nadine Wehmeier, Gerd Fischer, Sandra Herlufsen, Franziska Wolny, Matthias Wagner, Karsten Bothe, and Matthias Müller

***Abstract*—We investigate the degradation and regeneration behavior of quasi-monocrystalline silicon passivated emitter and rear cells under illumination at elevated temperatures. The decrease and increase of the solar cell efficiencies over time is accelerated under increased temperature or illumination intensity. We examine the defect activation kinetics and determine rate constants both for the degradation and regeneration. We apply temperatures in the range of 37–140 °C and illumination intensities in the range of 0.1–1.4 suns. These conditions typically occur when operating solar modules in the field. The rate constants are strongly increased with increasing temperature and increasing illumination intensity. We perform multiple regressions fits of the degradation and regeneration data with different approaches for the illumination intensity dependence. A linear illumination intensity dependence on the rates of degradation and regeneration is found. Activation energies for the degradation and regeneration of (0.89 ± 0.04) eV and (1.07 ± 0.07) eV, respectively, are extracted that allow for identification of the defect activation and deactivation mechanisms.**

***Index Terms*—Defect activation kinetics, light and elevated temperature induced degradation (LeTID), quasi-monocrystalline silicon (QM-Si) passivated emitter and rear cells (PERC) solar cells, regeneration.**

I. Introduction

LIGHT and elevated temperature induced degradation (LeTID) was firstly described for multicrystalline silicon (mc-Si) passivated emitter and rear cells (PERC) solar cells in 2012 [1]. The root cause of the degradation mechanism is still unclear, but related to a bulk defect [2]. LeTID is thought to be related to the amount of hydrogen introduced into the wafer bulk [3]–[7]. A hydrogen induced defect is thus proposed as a possible origin of LeTID [8].

A correlation between LeTID defect density and hydrogen content in silicon nitride (SiN_x) changed by the SiN_x thickness is reported [9]. However, no link between LeTID strength and SiN_x hydrogen concentration is found recently [10]. The LeTID strength depends on the plasma enhanced chemical vapor deposition time and temperature of the SiN_x passivation layer [10]. Other studies indicate that additionally, the involvement of possibly metallic impurities plays a role for the defect generation and defect change [11], [12], [13], [14]. Thus, also other silicon wafer materials than mc-Si, like Czochralski-grown silicon (Cz-Si) [15] and cast-mono-Si [16] can be affected.

The kinetics of defect formation and regeneration is also observed in modules under outdoor conditions and takes about 3–4 years for degradation maximum in warm climate (Cyprus) [17] with a relative degradation of about 7%. The regeneration is expected to take up the full service life of a solar module. Thus, kinetic parameters of defect formation and regeneration are important to project energy delivered during the service life of solar modules under operating conditions. Additionally, kinetic parameters might improve the understanding of the defect itself.

Defect formation shows two processes with a slow and a fast component [18] in mc-Si material. The slow component is also studied by other authors for different materials [19], [20], [21], [22]. The defect activation is shown to be charge carrier injection-dependent [23] and follow in general linear behavior [23], [18]. The regeneration process is often observed [24] and investigated [19], [21]. The kinetics of the regeneration show an injection-dependence. Kersten *et al.* showed a different regeneration kinetic keeping PERC solar cells and modules in maximum power point or open-circuit operation [24]. Available activation energies for degradation $E_{a,degr}$ and regeneration $E_{a,reg}$ are summarized in Table I.

In this work, we study the degradation and regeneration kinetics in quasi-monocrystalline silicon (QM-Si) PERC cells under different illumination and temperature conditions on a time scale of up to about 15 000 h. We present a parameterization for both the degradation and the regeneration process, while so far mostly the degradation is discussed in the literature. By

Manuscript received January 29, 2021; revised March 10, 2021; accepted March 10, 2021. This work was supported by the German State of Lower Saxony and the German Federal Ministry of Economics and Energy and by industry partners within the research project "HELENE" under Contract 0325777C. *(Corresponding authors: Nadine Wehmeier; Gerd Fischer.)*

Nadine Wehmeier and Karsten Bothe are with the Institute for Solar Energy Research Hamelin, 31860 Emmerthal, Germany (e-mail: wehmeier@isfh.de; k.bothe@isfh.de).

Sandra Herlufsen was with the Institute for Solar Energy Research Hamelin, 31860 Emmerthal, Germany. She is now with the Hermes Germany GmbH, 22419 Hamburg, Germany (e-mail: sandra.herlufsen@hermesworld.com).

Gerd Fischer, Franziska Wolny, Matthias Wagner, and Matthias Müller were with the SolarWorld Innovations GmbH, 09599 Freiberg, Germany. They are now with the HSZG, 02763 Zittau, Germany, with the Fraunhofer IPMS, 01109 Dresden, Germany, with the Carl Zeiss SMT GmbH, 73447 Oberkochen, Germany, and also with the TU Freiberg, 09599 Freiberg, Germany (e-mail: gerd.fischer@hszg.de; franziska.wolny@ipms.fraunhofer.de; mtwagnerfg@posteo.de; matth.mueller@physik.tu-freiberg.de).

Color versions of one or more figures in this article are available at https://doi.org/10.1109/JPHOTOV.2021.3066239.

Digital Object Identifier 10.1109/JPHOTOV.2021.3066239

TABLE I
KINETIC PARAMETERS OF DEFECT FORMATION FOR DIFFERENT SILICON MATERIALS

Author	Ref.	Material	$E_{a,degr}$ [eV]	$E_{a,reg}$ [eV]
Bredemeier et al.	[18]	p-type mc	0.94 ± 0.06*	-
Vargas et al.	[19]	p-type mc	1.08 ± 0.05	1.11 ± 0.04
Liu et al.	[20]	p-type mc	0.62 - 0.78**	0.67 - 0.78**
Chen et al.	[21]	p-type mc, n-type Cz	0.70 ± 0.05	0.83 ± 0.15
Graf et al.	[22]	p-type FZ	0.78 ± 0.09	-

*Slow component with pre-exponential factors κ_0 is 9.37×10^8 s^{-1} at 0.5 suns.
**Derived by high intensity illumination in the range 14.6–74.5 kW/m² and in the temperature range from 100–200 °C.

combined fitting of the degradation and regeneration data, we extract a set of parameters that allows for prediction of the long-term behavior of QM-Si PERC cells and solar modules. We compare our resulting kinetic parameters to literature data for different silicon materials and find agreements that might indicate same root causes for LeTID in QM-Si and mc-Si.

II. EXPERIMENT

For the fabrication of the passivated emitter and rear cells (PERC), 15.6 × 15.6 cm² *p*-type boron-doped quasi-monocrystalline silicon (QM-Si) [25] wafers from one center brick with a resistivity of 1.7 Ωcm and an oxygen content of 1–2 × 10^{17} cm^{-3} are used for all investigated cells. The cell fabrication is performed both at SolarWorld Innovations (SWIN) [26] and at the Institute for Solar Energy Research Hamelin (ISFH) in order to investigate the influence of the processing. Fig. 1 shows the QM-Si PERC solar cells and the processing steps at SWIN and ISFH.

At SWIN, the wafers are subjected to a saw-damage removal and cleaning before the rear side is passivated with a SiO_xN_y/SiN_x stack. In the following texturing step, only the front side is textured. A standard $POCl_3$-diffusion is carried out to form the front side n^+-emitter. At the rear side, laser contact opening (LCO) is performed. A selective emitter (SE) is implemented by laser doping before the phosphosilicate glass (PSG) is removed and an emitter oxidation is carried out. A SiN_x layer is deposited on the front side that acts both as passivation and antireflective coating. The cells are metalized by Ag screen-printing on the front side and full-area Al screen-printing on the rear side. Cofiring in a belt furnace at a set peak temperature of 865 °C finalizes the cells and forms the Al-p^+-areas on the rear side [27].

At ISFH, the wafer cleaning is performed using an inline-tool (Rena BatchLab). A rear side protection layer is applied before texturing and diffusion. The front side n^+-emitter is formed during a $POCl_3$ phosphorus furnace diffusion. After the removal of the PSG and the dielectric protection layer, the rear side is passivated by aluminum oxide (AlO_y) using atomic layer deposition. On both sides a SiN_x passivation layer is applied. After LCO, the cells are metalized by screen-printing and co-firing in a belt furnace at a set peak temperature of 860 °C is applied.

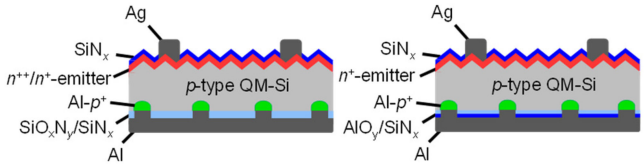

SWIN *p*-type QM-Si PERC	ISFH *p*-type QM-Si PERC
SDR+cleaning	SDR+cleaning
Rear: SiO_xN_y/SiN_x passivation	Rear: Protection layer
Front: Texturing	Front: Texturing
$POCl_3$-diffusion	$POCl_3$-diffusion
Laser contact opening	
Laser doping for SE-formation	
PSG removal	PSG+dielectric etch
Emitter oxidation	
	Rear: AlO_y+SiN_x passivation
Front: SiN_x passivation+ARC	Front: SiN_x passivation+ARC
	Laser contact opening
Front: Ag screen-printing	Front: Ag screen-printing
Rear: Al screen-printing	Rear: Al screen-printing
Co-firing	Co-firing

Fig. 1. Schematic of the finalized QM-Si PERC solar cells and the steps of the cell processing at SWIN and ISFH.

The cells are illuminated at light intensities between 0.12 and 1.4 suns applying halogen lamps and varying the distance between lamp and sample. The illumination intensity is measured using a calibrated float-zone reference cell with a measurement uncertainty of $6\%_{rel}$. In order to keep constant cell temperatures of 100 and 140 °C, the samples are put on a hot plate. For lower set temperatures of 37, 60, and 75 °C, the cells are heated by the halogen lamps and need to be cooled using a fan. The temperatures on the samples are measured using a thermocouple (type K).

The IV-parameters of the cells are measured using a LOANA cell tester (PV-tools).

III. RESULTS

A. LeTID and Regeneration of the Cell Efficiencies

Fig. 2 shows the normalized cell efficiencies of SWIN QM-Si PERC cells in dependence of the illumination time for four different parameter combinations. For each combination of temperature and illumination intensity, two cells are measured.

For all cells processed at SWIN, a degradation of the cell efficiency with increasing illumination time is observed that is considered to be a LeTID. The minimum cell efficiency and the time, after which the fully degraded state is reached, depends on the temperature and the illumination intensity. The fastest degradation is observed for the highest temperature of 140 °C, while for the lowest temperature of 37 °C, the degradation takes much longer and is more pronounced. If the cells are

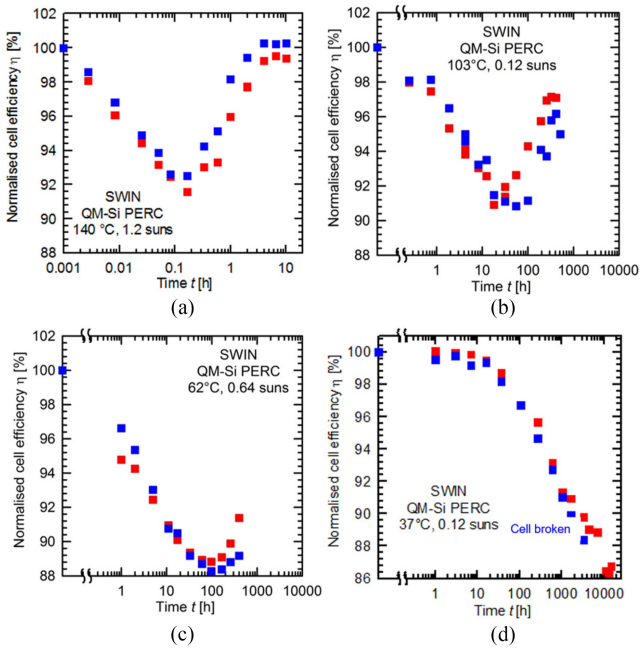

Fig. 2. Normalized efficiencies for QM-Si PERC processed at SWIN for temperatures between 37 and 140 °C and for different illumination intensities in the range of 0.1–1.2 suns. A pronounced degradation of the cell efficiencies followed by a regeneration is observed.

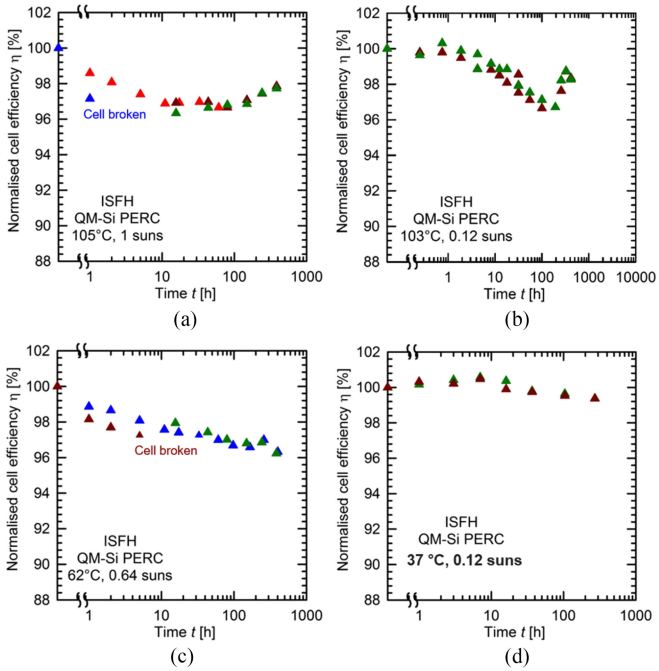

Fig. 3. Normalized efficiencies for QM-Si PERC processed at ISFH for temperatures between 37 and 105 °C and for different illumination intensities of 0.1–1.0 suns. Only a slight degradation and regeneration behavior is observed.

further illuminated and heated, the efficiencies recover. This regeneration process is slower than the degradation process (note the logarithmic scale in Fig. 2). For the lowest temperature of 37 °C, the regeneration is expected to start after about 15 000 h of illumination and is not measured.

In parallel, the QM-Si PERC cells processed at ISFH are exposed to identic or similar illumination and temperature conditions at the same test setup. The normalized cell efficiencies of ISFH QM-Si PERC cells are shown in Fig. 3.

For all applied illumination intensities and temperatures, the ISFH PERC cells show almost constant efficiencies (for 37 °C) or only a slight degradation and regeneration behavior (for about 100 °C) over the illumination time.

B. Rate Constants and Activation Energies

In the following, only the measured solar cell efficiencies of the SWIN QM-Si PERC cells are employed for the study of the degradation and regeneration kinetics. The inverse normalized cell efficiency is considered to be proportional to a normalized defect concentration N^*. Similar to [28], N^* is defined as

$$N^*(t) = \frac{1}{\eta_{\mathrm{norm}}(t)} - \frac{1}{\eta_{\mathrm{norm}}(t=0)} = \frac{1}{\eta_{\mathrm{norm}}(t)} - 1. \quad (1)$$

It allows for a quick estimation of the efficiency development in typical operating conditions for these QM-Si PERC cells. However, we would like to note that this method shows the following drawbacks: 1) no constant injection density [29] is applicable during the degradation and regeneration cycle and 2) no exact injection density is known for which the defect kinetic parameters are derived.

The experimental results indicate that the degradation and regeneration are two consecutive elementary steps that form an intermediate, recombination-active defect with a normalized defect concentration N^*. Therefore, we assume a simplified three-state-defect-model to describe N^*(t) behavior. An initial state A is transferred into a recombination-active state B with defect density N^*, which transfers into a nonrecombination-active defect state C. Thus, as soon as state B is formed, the regeneration reaction takes place simultaneously. The degradation and regeneration of the cell efficiencies and thus N^*(t) can be described by two superimposed exponential functions

$$N^*(t) = a_{\mathrm{deg}} \cdot R_{\mathrm{gen,deg}} \cdot \frac{\left(\exp\left(-R_{\mathrm{gen,deg}} \cdot t\right) - \exp\left(-R_{\mathrm{gen,reg}} \cdot t\right)\right)}{R_{\mathrm{gen,reg}} - R_{\mathrm{gen,deg}}}. \quad (2)$$

From an exponential fit, as shown in Fig. 4, the rate constants R_{gen} are derived both for the degradation $R_{\mathrm{gen,deg}}$ and for the regeneration $R_{\mathrm{gen,reg}}$. (The fit results for all SWIN PERC cells are summarized in Tables III and IV in the Appendix.)

The reverse reactions are considered to be slow compared to the investigated reactions. Both for the degradation and for the regeneration, the rate constants increase with increasing temperature and with increasing light intensity. The prefactor a_{deg} determines the maximum defect concentration. A mean value of $a_{\mathrm{deg}} = 10.9\% \pm 2.6\%$ is determined for all samples as an average maximal attainable efficiency degradation.

R_{gen} can be described with an Arrhenius equation

$$R_{\mathrm{gen}}(T) = \kappa_0 \cdot \exp\left(-\frac{E_{\mathrm{a}}}{k_{\mathrm{B}} \cdot T}\right). \quad (3)$$

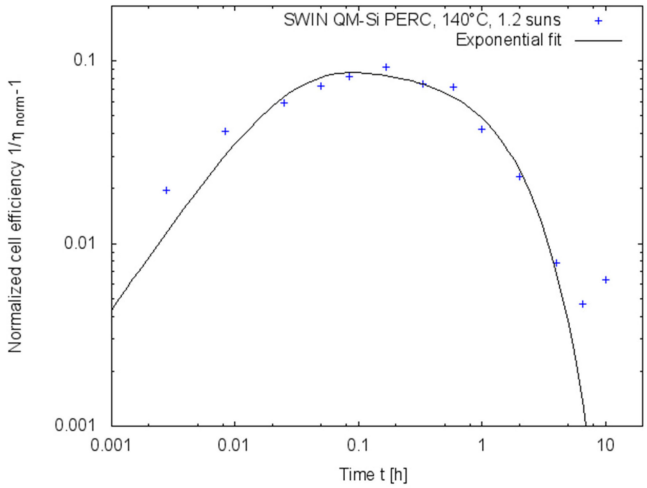

Fig. 4. Exponential fit of the inverse normalized cell efficiency to derive the rate constants for both the degradation and the regeneration, exemplarily shown for a PERC cell exposed to 140 °C and 1.2 suns [compare Fig. 2(a)].

The pre-exponential factor κ_0 is the attempt frequency, $k_\mathrm{B} = 8.617 \times 10^{-5}$ eV/K is the Boltzmann constant and E_a is the activation energy for the defect generation and annihilation, respectively.

A regression fit of the degradation and regeneration rate constants based on the Arrhenius equation, see (3), is performed with the assumption that the attempt frequency $\kappa_0(I)$ is dependent on the illumination intensity I but independent on the temperature T while the exponential function has a strong temperature dependence but is constant for different light intensities. We motivate the introduction of $\kappa_0(I)$ by the latest observations that the rate constants depend (linearly) on carrier injection [18], [23], [24].

In order to ensure this, three approaches of multiple regressions were applied to the logarithmic form of the Arrhenius equation

$$\ln\,[R_\mathrm{gen}\,(T,I)] = \ln[\kappa_0\,(I)] - \frac{E_\mathrm{a}}{k_\mathrm{B}\cdot T}. \tag{4}$$

1) The illumination intensity is treated as an independent categorical factor [30] [see Fig. 5(a) and (b)].
2) To ensure a nonexponential dependency of the rate constants from the illumination intensity, the natural logarithm of the illumination intensity is treated as a scalar predictor in the regression [in Fig. 5(c) and (d)].
3) This approach corresponds to 2). However, to attain a strict linear dependency of the rate constants from the illumination intensity, the prefactor of the illumination intensity has been fixed to 1 in the regression.

For the multiple regressions of approaches 2) and 3), (5) is used where $E_\mathrm{a} = a_3/k_\mathrm{B}$

$$\ln\,[R_\mathrm{gen}] = \ln[a_1] + a_2 \ln[I] - \frac{a_3}{T}. \tag{5}$$

The pre-exponential factor is

$$\kappa_0 = \exp\left(\ln[a_1] + a_2 \ln[I]\right) = a_1 \cdot I^{a_2}. \tag{6}$$

TABLE II
RESULTS OF THE DIFFERENT REGRESSION APPROACHES

Process / Approach	a_1 [10^8/s/suns]	a_2	E_a [eV]
Degradation / 1)	Cat. factor*	Cat. factor*	0.85 ± 0.08
Degradation / 2)	9.17 ± 12.45	0.98 ± 0.15	0.89 ± 0.05
Degradation / 3)	8.55 ± 9.57	1	0.89 ± 0.04
Regeneration /1)	Cat. factor*	Cat. factor*	0.84 ± 0.14
Regeneration / 2)	14.00 ± 30.57	1.05 ± 0.18	1.06 ± 0.08
Regeneration / 3)	17.94 ± 35.58	1	1.07 ± 0.07

*Categorical factor derived in multiple regressions, as shown in Fig. 5, corresponds to pre-exponential factor κ_0 as in (4).

From the regression fits for the degradation and regeneration shown in Fig. 5, activation energies are derived and listed in Table II

For the degradation in the categorical approach, the attempt frequency increases linearly with increasing light intensity up to 0.6 suns. For higher intensities up to 1.2 suns, a saturation behavior of κ_0, and thus, of the rate constant $R_\mathrm{gen,deg}$ is observed. In case of the regeneration in the categorical approach, the attempt frequency increases continuously with increasing light intensity.

For the regression approach using (5), the scalar predictor a_2 is derived to 0.98 ± 0.15 and 1.05 ± 0.18 for degradation and regeneration, respectively. Both values are very close to one, suggesting that a linear dependence between the rate constants and the illumination exist for degradation and regeneration. Thus, the regression with fixed $a_2 = 1$ shows very similar results and is not additionally shown in additional figures.

The derived activation energies E_a for the degradation process of 0.85 to 0.89 eV are for all three approaches in agreement within the derived uncertainty, although different behavior of the pre-exponential factor κ_0 in dependence of I is assumed. For the regeneration process, the activation energy derived from approaches 2) and 3) with a linear dependence of the pre-exponential factor κ_0 from I of 1.06 and 1.07 eV are in agreement within the measurement uncertainty. The categorical approach 1) leads to a slightly lower activation energy with an increased uncertainty of $E_\mathrm{a} = 0.84 \pm 0.14$ eV, which results from the variation in the regeneration data [compare Fig. 5 (b)] and higher number of free fit parameters of the categorical regression.

IV. DISCUSSION

From QM-Si wafers, PERC solar cells were fabricated by two different process sequences. The ISFH PERC cells showed almost constant efficiencies for all applied illumination intensities and temperatures whereas SWIN cells showed pronounced degradation and regeneration. The reason lies in the different processing sequence at ISFH and at SWIN. Especially the firing step can be adapted to allow for a reduced level of LeTID or even a complete avoidance of the degradation: Bredemeier *et al.* reported that for a reduced set peak firing temperature of 650 °C, the carrier lifetime is constant under illumination and temperature while for 900 °C, a pronounced degradation

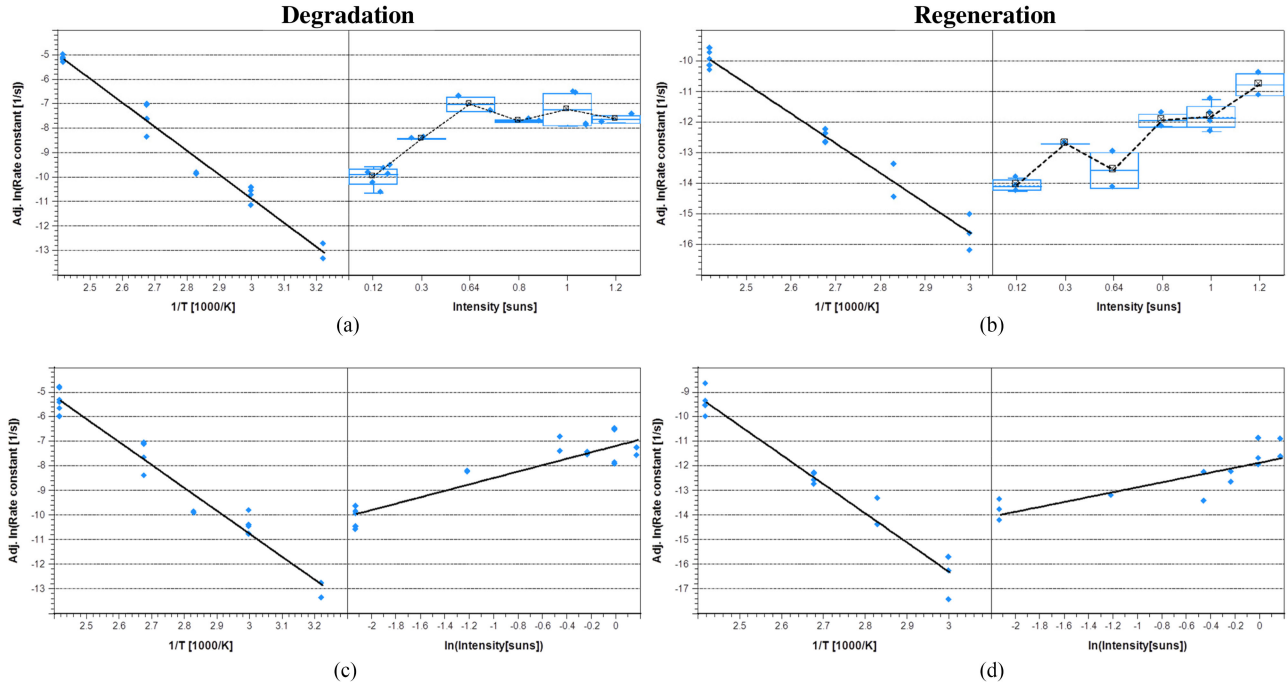

Fig. 5. Multiple regressions of the rate constants for degradation (a), (c) and regeneration (b), (d) of the investigated SWIN QM-Si PERC solar cells. Approach 1) is shown in (a) and (b): the adjusted Arrhenius plot (inside left) and the illumination intensity (inside right) as categorical factor. Approach 2) is shown in (c) and (d): the adjusted Arrhenius plot and the natural logarithm of illumination intensity as scalar predictor.

of mc-Si lifetime samples and increased defect densities are observed [11], [31]. In addition, Eberle *et al.* and Sen *et al.* indicated an influence of the ramp-up and cool-down rates of different firing temperature profiles on the degradation behavior [13], [32].

The ISFH PERC solar cells were fired in a belt furnace with a firing temperature profile resulting in a measured maximum sample temperature of about 750 °C for a set peak temperature of 860 °C [31]. In contrast, for the SWIN PERC cells, higher actual sample temperatures of about 840 °C were reached despite the similar set peak temperature of 865 °C due to the larger dimension and thermal capacity of the belt furnace. Thus, the about 90 K lower actual peak temperature allowed to decrease the level of LeTID on the ISFH cells. For the SWIN cells, we could observe a pronounced degradation and regeneration behavior of the cell efficiencies that could be parameterized.

Kinetic defect behavior was therefore studied on the SWIN PERC solar cells. Simultaneous regeneration right after beginning degradation was observed, which could be described by a simplified three-state defect model. Thus, only the combined fitting of the degradation and regeneration behavior of the normalized cell efficiency by two superimposed exponential functions successfully led to rates for further investigations and a rather stable maximal attainable efficiency degradation of 10.9% $\pm$ 2.6% for the full set of investigated QM-Si PERC cells, which became visible at low temperature and low illumination intensity treatment. By the determined activation energies and attempt frequencies, the mechanism of the degradation and regeneration in our investigated QM-Si PERC cells was characterized.

The three different strategies of multiple regressions of the temperature- and illumination-dependent rates of degradation and regeneration showed in general similar results supporting strongly the linear intensity dependence of the rates for both degradation and regeneration in the range of investigated conditions. The fit parameter a_2 includes well the value of one within its uncertainty (regression approach 2). Thus, we assume that the processes were driven by the change of the carrier injection density applicable within the solar cell [23], [24], which approximately scales linearly with illumination intensity. Therefore, we consider the results of the regression approach 3) as the most reasonable and suitable.

For the degradation process, we identified LeTID as the root cause by comparing our resulting kinetic parameters to literature data: For the formation of boron-oxygen (B-O) related recombination centers that lead to a carrier lifetime degradation in B-doped monocrystalline Cz-Si, Bothe *et al.* observed a fast initial and a slow degradation. For the slow degradation, an activation energy of $E_a = (0.475 \pm 0.035)$ eV and an attempt frequency of $\kappa_0 = (4 \times 10^3 - 1 \times 10^5)$ s^{-1} that depends on the boron concentration was reported in [33]. The light-induced carrier lifetime degradation in mc-Si was investigated by Bredemeier *et al.* They observed a fast and a slow component of the lifetime degradation and report an activation energy of $E_a = (0.94 \pm 0.06)$ eV for the slow component [18]. They found a linear dependence of the degradation rate constant on the illumination intensity in [11]. The observed behavior of our investigated QM-Si PERC cells was explained by LeTID, which can clearly be distinguished from B-O [33], additionally by the low oxygen content in QM wafers, or iron-boron [34] related degradation by the different degradation and regeneration kinetic characteristics, as you see from Table II. Our determined activation energy for the degradation $E_a = (0.89 \pm 0.04)$ eV is in agreement

within the measurement uncertainty with the activation energies reported by Bredemeier for mc-Si [18] (see Table I). This might indicate that the same degradation mechanism is responsible both for the efficiency degradation in QM-Si PERC cells and the lifetime degradation in mc-Si carrier lifetime samples. As a consequence, the degradation cannot be explained by recombination at crystallographic defects such as grain boundaries because in QM-Si wafers from the center bricks, no grains are present. It supports the finding by Chen *et al.* [15] for *n*-type silicon wafers where also no grains were present, although LeTID is observed.

The root cause for the degradation of our QM-Si PERC cells might be hydrogen that diffused from the hydrogen-rich SiN_x passivation layer into the silicon bulk during firing, as proposed for carrier lifetime samples [35]. Additionally, one or more metallic impurities might be involved in a defect formation that occurs during firing under certain firing conditions [11], [12]. We could demonstrate that for a firing process with a reduced actual peak temperature the degradation mechanism could be suppressed, and thus LeTID-free PERC solar cells could be fabricated from our *p*-type QM-Si material.

For the regeneration process only few studies are available. We determined an activation energy of (1.07 $\pm$ 0.07) eV, which matches the work of Vargas *et al.* [19] within its uncertainty (see Table I). However, we could not confirm the similarity between the activation energies of the degradation and regeneration processes as stated by Vargas *et al.* [19]. The activation energy reported by Liu *et al.* [20] is much lower than the one derived within our work, which might originate by the high illumination intensity and temperatures used by Liu *et al.* within their work.

By the derived attempt frequencies and activation energies, a complete parameter set is available and could be used to describe service lifetime kinetics of the LeTID defect in solar modules based on similar *p*-type QM-Si PERC cells.

V. Conclusion

The LeTID defect is investigated in QM-Si PERC cells. Combined fitting of two superimposed exponential functions to the normalized cell efficiency, showing degradation and regeneration, is carried out for cell temperatures in the range of 37 to 140 °C and illumination intensities of 0.1 to 1.4 suns. Derived rates of degradation and regeneration increase with higher temperature and/or higher illumination intensities. They are used to determine attempt frequencies and activation energies for both processes. The rates are investigated by three different strategies of multiple regressions considering simultaneously temperature and illumination intensity where the pre-exponential factor is only assumed intensity dependent. Degradation and regeneration rates show a linear correlation to the illumination intensity in the investigated range. The degradation process has an activation energy of (0.89 $\pm$ 0.04) eV indicating that the LeTID on QM-Si shows comparable values to LeTID in multicrystalline silicon. The regeneration process has an activation energy of (1.07 $\pm$ 0.07) eV being also comparable to results determined for multicrystalline silicon.

A suitable set of attempt frequencies and activation energies, considering temperature and illumination influence, is derived to predict long-term behavior of the efficiencies of solar modules made from QM-Si PERC cells during their service life.

Appendix

TABLE III
Fit Results of the Rate Constants for the Degradation

PERC Cell Name	Temperature T [°C]	Intensity I [suns]	Rate consta R_{gen} [1/s]
SWIN21	37	0.12	5.6E-07
SWIN06	37	0.12	3.0E-07
SWIN27	60	0.12	5.5E-06
SWIN28	60	0.12	4.1E-06
SWIN01	100	0.12	9.1E-05
SWIN31	100	0.12	4.3E-05
SWIN15	140	0.3	5.0E-03
SWIN16	140	0.3	5.3E-03
SWIN08	60	0.64	9.4E-05
SWIN02	60	0.64	5.2E-05
SWIN13	140	0.8	1.0E-02
SWIN14	140	0.8	1.1E-02
SWIN03	80	1	1.5E-04
SWIN04	80	1	1.6E-04
SWIN20	100	1	2.5E-03
SWIN18	100	1	2.6E-03
SWIN11	140	1.2	1.3E-02
SWIN12	140	1.2	9.8E-03

TABLE IV
Fit Results of the Rate Constants for the Regeneration

PERC Cell Name	Temperature T [°C]	Intensity I [suns]	Rate constant R_{gen} [1/s]	Uncertainty [1/s]
SWIN21	37	0.12	n.a.	n.a.
SWIN06	37	0.12	n.a.	n.a.
SWIN27	60	0.12	n.a.	n.a.
SWIN28	60	0.12	3.2E-08	1.6E-08
SWIN01	100	0.12	9.8E-07	1.4E-07
SWIN31	100	0.12	6.2E-07	1.2E-07
SWIN15	140	0.3	n.a.	n.a.
SWIN16	140	0.3	3.7E-05	5.4E-06
SWIN08	60	0.64	9.7E-08	3.7E-08
SWIN02	60	0.64	3.0E-08	1.3E-08
SWIN13	140	0.8	9.9E-05	1.4E-05
SWIN14	140	0.8	6.5E-05	8.6E-06
SWIN03	80	1	2.9E-06	5.1E-07
SWIN04	80	1	9.9E-07	7.6E-07
SWIN20	100	1	7.9E-06	2.5E-06
SWIN18	100	1	6.0E-06	1.9E-06
SWIN11	140	1.2	1.8E-04	2.9E-05
SWIN12	140	1.2	3.7E-04	5.3E-05

REFERENCES

[1] K. Ramspeck *et al.*, "Light induced degradation of rear passivated mc-Si solar cells," in *Proc. 27th Eur. Photovolt. Sol. Energy Conf.*, pp. 861–865, 2012.

[2] K. Nakayashiki *et al.*, "Engineering solutions and root-cause analysis for light induced degradation in p-type multicrystalline silicon PERC modules," *IEEE J. Photovolt.*, vol. 6, no. 6, pp. 860–868, Jul. 2016.

[3] M. Jensen *et al.*, "Evaluating root cause: The distinct roles of hydrogen and firing in activating light and elevated temperature-induced degradation," *J. Appl. Phys.*, vol. 124, 2018, Art. no. 085701.

[4] T. Niewelt, F. Schindler, W. Kwapil, R. Eberle, J. Schoen, and M. C. Schubert, "Understanding the light-induced degradation at elevated temperatures: Similarities between multicrystalline and float zone p-type silicon," *Prog. Photovolt. Res. Appl.*, vol. 26, pp. 533–542, 2018.

[5] J. Schmidt, D. Bredemeier, and D. Walter, "On the defect physics behind light and elevated temperature-induced degradation (LeTID) of multicrystalline silicon solar cells," *IEEE J. Photovolt.*, vol. 9, no. 6, pp. 1497–1503, Nov. 2019.

[6] D. Chen *et al.*, "Hydrogen-induced degradation: Explaining the mechanism behind light and elevated temperature-induced degradation in n- and p-type silicon," *Sol. Energy Mater. Sol. Cells*, vol. 207, 2020, Art. no. 110353.

[7] U. Varshney *et al.*, "Controlling light- and elevated-temperature-induced degradation with thin film barrier layers," *IEEE J. Photovolt.*, vol. 10, no. 1, pp. 19–27, Jan. 2020.

[8] A. Ciesla *et al.*, "Hydrogen-induced degradation," in *Proc. 7th World Conf. Photovolt. Sol. Energy Conf.*, pp. 1–8, 2018.

[9] U. Varshney *et al.*, "Evaluating the impact of SiNx thickness on lifetime degradation in silicon," *IEEE J. Photovolt.*, vol. 9, no. 3, pp. 601–607, May 2019.

[10] J. Lindroos, A. Zuschlag, D. Skorka, and G. Hahn, "Silicon nitride deposition: impact on lifetime and light-induced degradation at elevated temperature in multicrystalline silicon," *IEEE J. Photovolt.*, vol. 10, no. 1, pp. 8–18, Jan. 2019.

[11] D. Bredemeier, D. Walter, S. Herlufsen, and J. Schmidt, "Lifetime degradation and regeneration in multicrystalline silicon under illumination at elevated temperature," *AIP Adv.*, vol. 6, 2016, Art. no. 035119.

[12] D. Bredemeier, D. Walter, and J. Schmidt, "Possible candidates for impurities in mc-Si wafers responsible for light-induced lifetime degradation and regeneration," *Sol. RRL*, vol. 2, 2017, Art. no. 1700159.

[13] R. Eberle, W. Kwapil, F. Schindler, S. W. Glunz, and M. C. Schubert, "Firing temperature profile impact on light induced degradation in multicrystalline silicon," *Energy Procedia*, vol. 124, pp. 712–717, 2017.

[14] M. Wagner *et al.*, "Correlation of the LeTID amplitude to the aluminium bulk concentration and oxygen precipitation in PERC solar cells," *Sol. Energy Mater. Sol. Cells*, vol. 187, pp. 176–188, 2018.

[15] D. Chen *et al.*, "Evidence of an identical firing-activated carrier-induced defect in monocrystalline and multicrystalline silicon," *Sol. Energy Mater. Sol. Cells*, vol. 172, pp. 293–300, 2017.

[16] H. C. Sio *et al.*, "Light and elevated temperature induced degradation in p-type and n-type cast-grown multicrystalline and mono-like silicon," *Sol. Energy Mater. Sol. Cells*, vol. 182, pp. 98–104, 2018.

[17] F. Kersten *et al.*, "Performance loss induced by LeTID in the field," in *Proc. 33rd Eur. Photovoltaic Sol. Energy Conf. Exhib.*, pp. 25–29, 2017.

[18] D. Bredemeier, D. Walter, and J. Schmidt, "Light-induced lifetime degradation in high-performance multicrystalline silicon: Detailed kinetics of the defect activation," *Sol. Energ. Mat. Sol. Cells*, vol. 173, pp. 2–5, 2017.

[19] C. Vargas, G. Coletti, C. Chan, D. Payne, and Z. Hameiri, "On the impact of dark annealing and room temperature illumination on p-type multicrystalline silicon wafers," *Sol. Energy Mater. Sol. Cells*, vol. 189, pp. 166–174, 2019.

[20] Liu *et al.*, "Investigation of temperature and illumination dependencies of carrier-induced degradation in p-type multi-crystalline silicon," in *Proc. AIP Conf. Proc. 1999*, 2018, pp. 130014-1–130014-8.

[21] D. Chen *et al.*, "Hydrogen-induced degradation: Explaining the mechanism behind light and elevated temperature-induced degradation in n- and p-type silicon," *Sol. Energy Mater. Sol. Cells*, vol. 207, 2020, Art. no. 110353.

[22] A. Graf, A. Herguth, and G. Hahn, "Determination of BO-LID and LeTID related activation energies in Cz-Si and FZ-Si using constant injection conditions," in *Proc. AIP Conf. Proc.*, 2019, pp. 140003-1–140003-5.

[23] W. Kwapil, T. Niewelt, and M. C. Schubert, "Kinetics of carrier-induced degradation at elevated temperature in multicrystalline silicon solar cells," *Sol. Energy Mater. Sol. Cells*, vol. 173, pp. 80–84, 2017.

[24] F. Kersten *et al.*, "Degradation of multicrystalline silicon solar cells and modules after illumination at elevated temperature," *Sol. Energy Mater. Sol. Cells*, vol. 142, pp. 83–86, 2015.

[25] F. Wolny, A. Krause, M. Müller, G. Fischer, and H. Neuhaus, "Reduced metal contamination from crucible and coating using a silicon nitride based diffusion barrier for the growth of cast quasi-single crystalline silicon ingots," *J. Cryst. Growth*, vol. 514, pp. 49–53, 2019.

[26] P. Palinginis *et al.*, "Pioneering the industrialization of PERC technology: A review of the development of mono- and bifacial PERC solar cells at SolarWorld," *PV Int.*, vol. 42, pp. 51–72, Mar. 2019.

[27] M. Müller, F. Wolny, G. Fischer, A. Krause, P. Palinginis, and H. Neuhaus, "Change of the bulk carrier lifetime of high quality silicon wafers during PERC solar cell processing," in *Proc. 35th Eur. Photovoltaic Sol. Energy Conf. Exhib.*, 2018, pp. 366–370.

[28] S. Kim *et al.*, "Light-induced degradation and metastable-state recovery with reaction kinetics modeling in boron-doped Czochralski silicon solar cells," *Appl. Phys. Lett.*, vol. 105, 2014, Art. no. 083509.

[29] H. Hieslmair, "Time constants of degradation, regeneration, and destabilization of the B-O related defect," in *Proc. IEEE 43rd Photovoltaic Specialists Conf.*, 2016, pp. 0645–0650.

[30] *Cornerstone Users Guide*, Revision 7.2, camLine, Petershausen, Germany, 2020.

[31] D. Bredemeier, D. Walter, and J. Schmidt, "Lifetime degradation in multicrystalline silicon under illumination at elevated temperature: Indications for the involvement of hydrogen," in *Proc. AIP Conf. Proc. 1999*, 2018, pp. 130001-1–130001-7.

[32] C. Sen *et al.*, "Assessing the impact of thermal profiles on the elimination of light- and elevated-temperature-induced degradation," *IEEE J. Photovolt.*, vol. 9, no. 1, pp. 40–48, Jan. 2019.

[33] K. Bothe and J. Schmidt, "Electronically activated boron-oxygen-related recombination centers in crystalline silicon," *J. Appl. Phys.*, vol. 99, Jan. 2006, Art. no. 013701.

[34] A. Istratov, H. Hieslmair, and E. Weber, "Iron and its complexes in silicon," *Appl. Phys. A*, vol. 69, pp. 13–44, 1999.

[35] D. Bredemeier, D. Walter, R. Heller, and J. Schmidt, "Impact of hydrogen-rich silicon nitride material properties on light-induced lifetime degradation in multicrystalline silicon," *Phys. Statist. Sol. RRL*, vol. 13, 2019, Art. no. 1900201.